

Self-supervision is not magic: Understanding Data Augmentation in Image Anomaly Detection

Jaemin Yoo*

Tiancheng Zhao*

Leman Akoglu*

Abstract

Self-supervised learning (SSL) has emerged as a promising alternative to create supervisory signals to real-world tasks, avoiding the extensive cost of labeling. SSL is particularly attractive for unsupervised tasks such as anomaly detection (AD), where labeled anomalies are costly to secure, difficult to simulate, or even nonexistent. A large catalog of augmentation functions have been used for SSL-based AD (SSAD) on image data, and recent works have observed that the type of augmentation has a significant impact on performance. Motivated by those, this work sets out to put image-based SSAD under a larger lens and carefully investigate the role of data augmentation in AD through extensive experiments on three different models across 420 different tasks. Our main finding is that self-supervision acts as a yet-another model hyperparameter and should be chosen carefully in regard to the nature of true anomalies. That is, the alignment between data augmentation and the underlying anomaly-generating mechanism in given data is the key to the success of SSAD, and in the lack thereof, SSL even impairs (!) the accuracy. Moving beyond proposing another SSAD method, our study contributes to a better understanding of this growing area and lays out new directions for future research.

1 Introduction

Machine learning has made tremendous progress in creating models that can learn from carefully labeled data. However, the cost of high-quality labeled data is a major bottleneck for the future of this supervised learning paradigm. Most recently, self-supervised learning (SSL) has emerged as a promising alternative; *internally* generating some kind of supervisory signal to solve a task. In essence, an unsupervised task is transformed to a supervised problem by auto-generating labeled examples. This new paradigm has had great success in advancing NLP [6, 7] and has helped excel at various computer vision tasks [11]. Today, SSL is arguably the key toward “unlocking the dark matter of intelligence” [19].

SSL is particularly attractive for unsupervised tasks such as anomaly detection (AD), where labeled data is

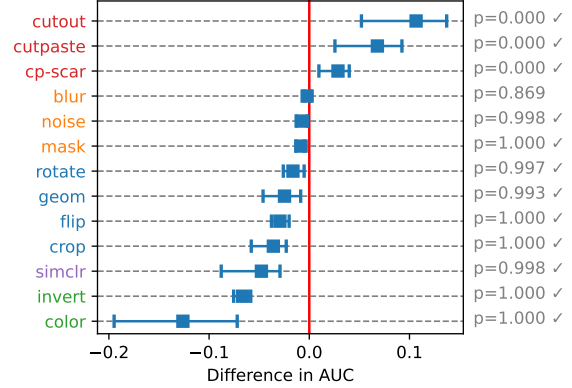


Figure 1: (best in color) Relative AUC of DAE in comparison to the vanilla AE on the controlled testbed with anomaly-generating function $\text{gen}:=\text{CutOut}$. Color in augmentation names denotes their categories. Local augmentations (in red) perform well thanks to the high alignment with gen , while others (e.g. in green) can even hurt (!) the accuracy significantly (p -values in gray). See our Key Finding 1 and 2 in Sec. 5.

rare or nonexistent, costly to obtain, or nontrivial to simulate in the face of unknown anomalies. As a result, the literature has seen a recent surge of SSL-based AD (SSAD) techniques [3, 5, 10, 20, 22, 26]. The common idea is incorporating “imaginary” or *pseudo* anomalies into the training and then separating inliers from these self/auto-generated anomalies. These pseudo anomalies are created in one of two ways: by transforming inliers via an augmentation function¹ or by “outlier-exposing” the training to external data sources [9, 16]. The former synthesizes new artificial samples, whereas the latter uses existing real ones from outside repositories.

While perhaps re-branding under the name SSL, the idea of injecting artificial anomalies to inlier data to create a labeled training set for AD dates back to the early 2000s [1, 27, 29]. Fundamentally, under the uninformative/uniform prior for the (unknown) anomaly-generating distribution, these methods are asymptotically consistent density level set estimators for the sup-

*Carnegie Mellon University (jaeminyoo@cmu.edu, tianchen@andrew.cmu.edu, lakoglu@andrew.cmu.edu).

¹E.g., rotate, blur, mask, color jitter, CutPaste [20], as well as “cocktail” augmentations GEOM [10] and SimCLR [4].

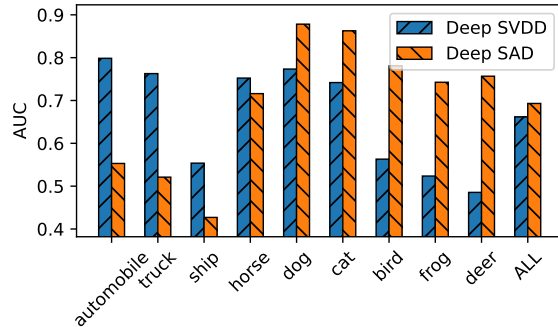


Figure 2: AUC distribution comparing DeepSAD with its no-SSL baseline, DeepSVDD, on CIFAR-10. We set Airplane as the normal class and use Rotate as aug. The x -labels represent the types of semantic anomalies. The self-supervision improves the average accuracy (the last column) but impairs accuracy on classes that are easily detected by unsupervised DeepSVDD. See Obs. 2.

port of the inlier data distribution [27]. Unfortunately, they are ineffective and sample-inefficient in high dimensions as they require a massive number of sampled anomalies to properly fill the sample space.

With today’s SSL methods for AD, we observe a shift toward various different, *non-uniform* priors on the distribution of anomalies. In fact, current literature on SSAD is laden with many different forms of generating pseudo anomalies, each introducing its own inductive bias. As a consequence, the success on any given AD dataset depends on which augmentation function is used or which external dataset the learning is exposed to as pseudo anomalies, and importantly “to what extent the pseudo anomalies mimic the nature of the true (yet unknown) anomalies” in the test data.

Not surprisingly, there exist evidences in the literature that the choice has a significant impact on the outcome. For example, Golan et al. [10] have shown that geometric transformations create better pseudo anomalies than pixel-wise augmentations for detecting semantic class anomalies. In contrast, Li et al. [20] have reported that (global) geometric transformations [10] fail at detecting small defects in industrial object images, where (local) augmentations such as random cut-and-paste perform significantly better (90.9 vs. 73.1 AUC on avg., see their Table 1). On semantic AD tasks, on the other hand, the *reverse* holds true (69.4 vs. 91.3 AUC, see their Sec. 5.4). Qiu et al. [22] have shown that even when learning a data augmentation function as a neural network, its hyperparameters should be tuned carefully for each task, which is in effect the same as choosing the function family of augmentations to use. Ye et al. [34] have observed that when pseudo anomalies are sampled from a biased subset of true anomalies, the detector’s errors become biased; the test error is lower on the seen

type of anomalies, at the expense of much larger error on unseen anomalies—even when unknown anomalies are easily detected by an *unsupervised* detector (!).

While partially reported evidence exists, the current literature lacks systematic scrutiny of the working assumptions for SSAD, where it is typical of the community to leave hyperparameter selection or their SSL design choices unjustified. Owing to task-dependent success, it is common to see different choices being made for different datasets in the same paper; e.g. a different outlier-exposure dataset per task is used in [9, 16], using medical outlier-exposure data for medical AD tasks while using (cut-mix) augmentation on other datasets in [9], to name just a few examples.

Motivated by these recent developments, this work sets out to put SSAD under a larger investigative lens. Our goal is to expose pitfalls and bring clarity and an improved understanding to the growing field of SSL for AD. Our contributions are summarized as follows:

- **Large-scale study of SSL on Image AD:** Through an extensive evaluation study, we answer the following: How do different choices for pseudo anomaly generation impact AD performance? Can data augmentation *degrade* performance? What is the key contributor to the success or the failure of SSL on image AD? We conduct numerous experiments on controlled testbeds as well as in-the-wild image datasets, using SSAD methods of three different types and across 420 different AD tasks.
- **Alignment between Pseudo & True Anomalies:** Our main finding is that self-supervision is *not* a “magic stick” for unsupervised AD, and remains to be a (yet-another) hyperparameter—the choice of which heavily influences the performance. The key factor is the alignment (or agreement) between the distributions generated by the data augmentation function aug versus the true anomaly-generating function gen (i.e., how well the pseudo anomalies mimic the true ones), where alarmingly, poor alignment even hurts accuracy (see Fig. 1) or leads to a biased error distribution (see Fig. 2).

To enable reproducibility and foster future research on SSL for AD, we open-source all testbeds and implementations in our study at <https://bit.ly/3SEti6t>.

2 Related Works

2.1 Generative Models Generative models learn the data distribution of normal examples and measure the anomaly score of an example based on its distance from the learned distribution. Generative models for AD include autoencoder-based models [38, 39], generative adversarial networks [2, 36], and flow-based models [14, 23]. Recent works [5, 33] proposed denoising au-

toencoder (DAE)-based models for SSAD by adopting domain-specific data augmentation functions instead of traditional Gaussian noise or Bernoulli masking [30, 31] to inject random noise to training data.

2.2 Classifier-based Models Augmentation prediction is to learn a classifier by creating pseudo labels of samples from multiple augmentation functions. The classifier network trained to differentiate augmentation functions is used to generate better representations of data. Many augmentation functions were proposed for anomaly detection in this sense, mostly for image data, including geometric transformation [10], random affine transformation [3], local image transformation [20], and learnable neural network-based transformation [22].

Outlier Exposure [9, 16] uses an auxiliary dataset as pseudo anomalies for training a classifier that separates it from normal samples. Since the choice of an auxiliary dataset has a large impact on the performance, previous works have chosen a suitable dataset for each target task considering the nature of true anomalies.

2.3 Semi-supervised Models Semi-supervised AD assumes that a few samples of true anomalies are given at training [25, 34]. Recently, Ye et al. [34] have shown that the observations from a biased subset of anomalies induce a bias in the model’s predictions, impairing its accuracy on unseen types of anomalies even when they are easy to detect by unsupervised models. Motivated by this, we understand semi-supervised AD as a form of self-supervised learning in that limited observations of (pseudo) anomalies play an essential role in accuracy, and it is essential to make a proper alignment between observations and the distribution of true anomalies.

3 Notations and Background

3.1 Notations We formally define the anomaly detection problem [5, 20, 22] as follows:

- **Given** a set $\mathcal{D} = \{\mathbf{x}_i\}_{i=1}^N$ of normal data, where N is the number of training samples, and $\mathbf{x}_i \in \mathbb{R}^d$.
- **Find** a score function $s(\cdot) \in \mathbb{R}^d \rightarrow \mathbb{R}^1$ such that $s(\mathbf{x}) < s(\mathbf{x}')$ if \mathbf{x} is normal and \mathbf{x}' is abnormal.

The definition of normality (or abnormality) of data is different for specific datasets and tasks. For the generality of notations, we introduce an anomaly-generating function $\text{gen}(\cdot) : \mathbb{R}^d \rightarrow \mathbb{R}^d$ that creates anomalies from normal data, and represent the nature of target anomalies with gen . We denote a test set associated with gen , containing both normal and abnormal data, as \mathcal{D}_{gen} .

Specifically, we aim at self-supervised anomaly detection (SSAD), which addresses the problem by learning a neural net model $f(\cdot; \theta) \in \mathbb{R}^d \rightarrow \mathbb{R}^h$ using a data augmentation function $\text{aug}(\cdot) \in \mathbb{R}^d \rightarrow \mathbb{R}^d$, where θ is the set of all learnable parameters in f , and defining a score function $s(\cdot)$ on top of the learned representations. We

denote a detector model trained with an augmentation function aug by f_{aug} when there is no ambiguity.

How aug is used for the training of f_{aug} depends on the type of f . We introduce three representative models from the three categories in Sec. 2, respectively.

3.2 DAE The objective function for a denoising autoencoder (DAE) [30] f_{aug} is given as follows:

$$(3.1) \quad l(\theta) = \sum_{\mathbf{x} \in \mathcal{D}} \|f(\text{aug}(\mathbf{x}); \theta) - \mathbf{x}\|_2^2.$$

That is, f_{aug} aims to reconstruct $\text{aug}(\mathbf{x})$ as the original \mathbf{x} . We use the mean squared error between \mathbf{x} and the reconstructed version $f(\mathbf{x}; \theta)$ as an anomaly score. The training of *vanilla* autoencoder (AE) models is done by employing the identity function $\text{aug}(\mathbf{x}) = \mathbf{x}$.

3.3 AP The objective function for an augmentation predictor (AP) [10] f_{aug} is given as follows:

$$(3.2) \quad l(\theta) = \sum_{\mathbf{x} \in \mathcal{D}} \sum_{k=1}^K \text{NLL}(f(\text{aug}_k(\mathbf{x}); \theta), k),$$

where K is the number of separable *classes* of aug , aug_k is the k -th class of aug , and $\text{NLL}(\hat{y}, y) = -\log \hat{y}_y$ is the negative log likelihood term. The set of separable classes is defined differently for each aug function: for example, image rotation [10] sets $K = 4$ and models each aug_k as the e -degree rotation with $e \in \{0, 90, 180, 270\}$, making f a 4-class classifier. Unlike DAE and DeepSAD, there is no *vanilla* model of AP that works without aug .

The idea to define the anomaly score of \mathbf{x} by AP is to compute $s(\mathbf{x}) = -\sum_{k=1}^K [f(\text{aug}_k(\mathbf{x}))]_k$, which means that \mathbf{x} gets a high score if its classification is failed. For the exact definition, refer to the original paper [10].

3.4 DeepSAD The objective function for DeepSAD [25] f_{aug} is given as follows:

$$(3.3) \quad l(\theta) = \sum_{\mathbf{x} \in \mathcal{D}} \|f(\mathbf{x}; \theta) - \mathbf{c}\| + \|f(\text{aug}(\mathbf{x}); \theta) - \mathbf{c}\|^{-1},$$

where the hypersphere center \mathbf{c} is set as the mean of the outputs obtained from an initial forward pass of the training data \mathcal{D} . The anomaly score of \mathbf{x} is defined as the distance between \mathbf{x} and \mathbf{c} , i.e., $\|\mathbf{x} - \mathbf{c}\|_2^2$. We adopt DeepSVDD [24] as the no-SSL baseline of DeepSAD by removing the second term in the training.

4 Experimental Setup

4.1 Models We conduct experiments on the three detector models introduced in Sec. 3: DAE, DeepSAD, and AP. We also include the no-SSL baselines AE and DeepSVDD for DAE and DeepSAD, respectively, with the same model architectures. Detailed information on the models is given in Appendix A.

Table 1: AUC of the three models on the CIFAR-10C and CIFAR-10 datasets; the first three gen functions are from CIFAR-10C, while Semantic means the anomalies of different semantic classes in CIFAR-10. Every model performs best when aug and gen are matched, supporting Key Finding 1. Different aug functions work best in Semantic, where the alignment with gen is not clear.

Model	Augment (= aug)	Anomaly functions (= gen)			
		CutOut	Flip	Invert	Semantic
DAE	CutOut	0.974	0.593	0.654	0.604
DAE	Flip	0.771	0.865	0.772	0.691
DAE	Invert	0.746	0.663	0.970	0.690
DAE	GEOM	0.813	0.726	0.724	0.621
DeepSAD	CutOut	0.999	0.580	0.556	0.592
DeepSAD	Flip	0.727	0.876	0.731	0.691
DeepSAD	Invert	0.674	0.659	0.973	0.695
DeepSAD	GEOM	0.938	0.758	0.699	0.682
AP	CutOut	0.797	0.503	0.508	0.505
AP	Flip	0.639	0.959	0.836	0.780
AP	Invert	0.645	0.717	0.994	0.753
AP	GEOM	0.760	0.944	0.881	0.863

4.2 Augmentation Functions We study various types of augmentation functions defined on the image domain, which are categorized into five groups. Bullet colors are the same as in Figs. 1, 3, and 4.

- Geometric: Crop [4], Rotate, Flip, & GEOM [10].
- Local: CutOut [8], CutPaste & CutPaste-scar [20].
- Elementwise: Blur [4], Noise, & Mask [31].
- Color-based: Invert & Color (jittering) [4].
- Mixed: SimCLR [4].

Geometric functions make global geometric changes to images such as by rotation or flipping. Local augmentations, in contrast, modify only a part of an image such as by erasing a small patch. Elementwise augmentations modify every pixel individually. Color-based functions change the color of images, while mixed augmentations combine multiple categories of augmentation functions. Detailed information is given in Appendix B.

4.3 Datasets Our experiments are conducted on two kinds of testbeds, containing 420 different tasks overall. The first is *in-the-wild* testbed, where a single semantic class is selected as normal and another class is selected as anomalous. We include four image datasets in this testbed: MNIST [18], FashionMNIST [32], SVHN [21], and CIFAR-10 [17]. Since all datasets have 10 different classes, we have 90 tasks corresponding to different pairs of normal and anomalous classes for each dataset.

The second is *controlled* testbed, where we adopt a known function as the anomaly-generating function gen to have full control of the anomalies. Given two datasets SVHN and CIFAR-10, we use three aug functions as gen : CutOut, Flip, and Invert, making 30 different tasks (10 classes \times 3 anomalies) for each dataset. We denote these

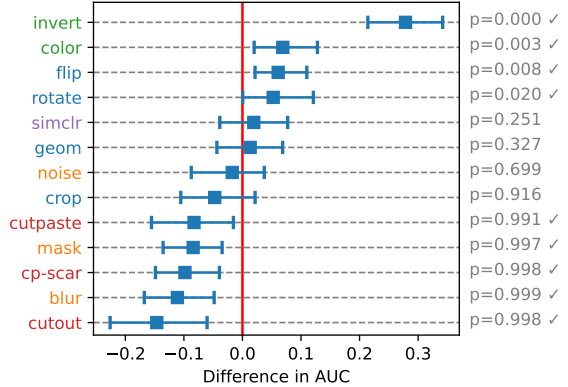


Figure 3: (best in color) Relative AUC of DeepSAD in comparison to DeepSVDD on the controlled testbed with $\text{gen} := \text{Invert}$. Color in augmentation names denotes the categories. Color-based augmentations (in green) work best due to the high alignment with gen , while others (e.g. in red) can even hurt the accuracy significantly (p -values in gray). See Key Finding 1 and 2.

datasets by SVHN-C and CIFAR-10C, respectively.

4.4 Evaluation Given a detector model f and a test set \mathcal{D}_{gen} containing both normal data and anomalies for each task, we define the score $r(\mathbf{x})$ of \mathbf{x} as the percentile of $s(\mathbf{x})$ in \mathcal{D}_{gen} . That is, \mathbf{x} is predicted as an anomaly if $s(\mathbf{x})$ is relatively high. We evaluate each f by measuring the area under the ROC curve (AUC) of scores.

We focus on the alignment between aug and gen in evaluation. In the controlled testbed, where both aug and gen are known, we compare the families of aug and gen and say that there is high alignment if they are from the same family, e.g., $\text{aug} := \text{Rotate}$ and $\text{gen} := \text{Flip}$, both of which are geometric augmentations. For the *in-the-wild* testbed, we measure Maximum Mean Discrepancy (MMD) [12] between two sets of images generated from aug and gen , respectively. Since the pixel-level distances in images are not matched with semantic differences, we use pretrained ResNet50 [15] to generate embeddings on which MMD is measured; this model is used only for the measurement, not in actual experiments for AD. Details on the exact definition of MMD are in Appendix C.

5 Success and Failure of Augmentation

5.1 Key Findings We investigate *when* augmentation succeeds or otherwise fails by comparing a variety of augmentation functions on the three models.

KEY FINDING 1. *Given \mathcal{D}_{gen} , f_{aug} outperforms $f_{\text{aug}'}$ if aug is better aligned with gen than aug' is.*

Table 1 supports Key Finding 1 by experiments on CIFAR-10C and CIFAR-10. In the controlled tasks with $\text{gen} \in \{\text{CutOut}, \text{Flip}, \text{Invert}\}$, $\text{aug} = \text{gen}$ performs best in all three models, even though the exact numbers are

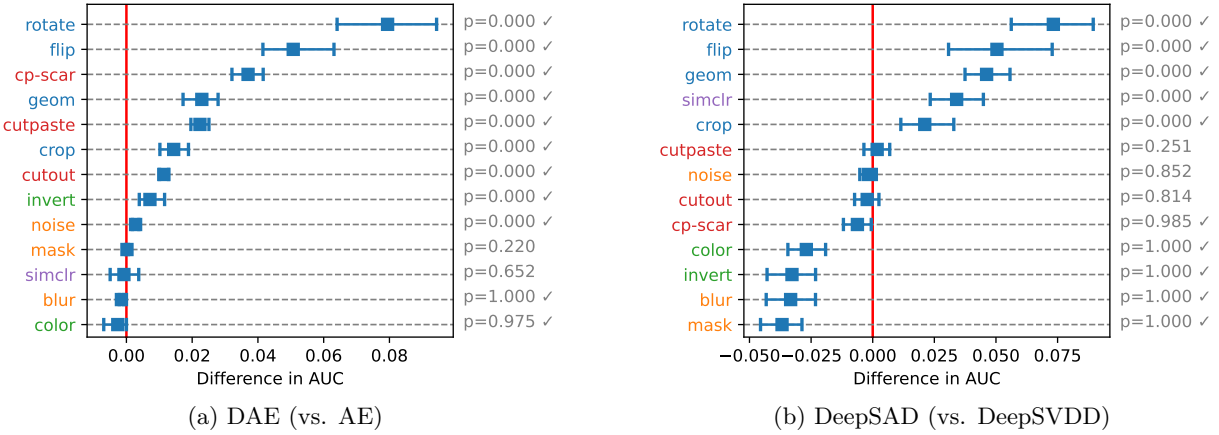


Figure 4: (best in color) Relative AUC on the in-the-wild testbed in which anomalies are different semantic classes. Color in augmentation names represents their categories. The geometric augmentations (in blue) perform best in both cases, improving the baselines, while others make insignificant changes or impair the baselines. See Obs. 1.

different based on the basic performances of models. On the other hand, for the semantic anomalies, different aug functions work best: Flip in DAE, GEOM in AP, and Invert in DeepSAD. This is because different semantic classes are hard to be represented by single aug , making no aug achieve the perfect alignment with gen . In such a case, different patterns are shown for different models: DAE shows similar performances with all aug , while AP shows clear strength with GEOM, as shown in [10].

KEY FINDING 2. *Given \mathcal{D}_{gen} , f_{aug} impairs the accuracy of f if the alignment between aug and gen is poor.*

We compare DAE and DeepSAD with their no-SSL baselines, AE and DeepSVDD, respectively, to see when augmentation helps or hurts the base accuracy. Recall that AP does not have such a baseline (see Sec. 3).

To that end, we conduct an experiment for all possible pairs of classes and then run the paired Wilcoxon signed-rank test [13] between f_{aug} and the vanilla f . We report the (pseudo) medians, 95% confidence intervals, and p -values as shown in Fig. 1. The x -axis means the relative AUC compared with that of the vanilla f . We consider that aug is beneficial (or harmful) if the p -value is smaller than 0.05 (or larger than 0.95).

Figs. 1 and 3 show the results of Wilcoxon tests on the controlled testbed by DAE and DeepSAD, respectively. Each row summarizes the AUCs from 20 tasks across two datasets (CIFAR-10C and SVHN-C) and ten classes each. In both figures, aug functions that exhibit the best alignment with gen significantly improve the accuracy of vanilla f : the local augmentations in Fig. 1, and the color-based augmentations in Fig. 3. On the other hand, the remaining aug functions make negligible changes or even cause a significant decrease in AUC, supporting Key Finding 2: the alignment between aug and gen determines the success or the failure of f_{aug} on

Table 2: MMD between augmented data and semantic anomalies on the in-the-wild testbed. The functions are sorted by the average distance. Geometric aug functions (in blue) show the smallest distances in general, consistently with the AUC results on Fig. 4.

Augment	MNIST	Fashion	CIFAR	SVHN	Average
• Rotate	1.831	1.855	0.267	0.186	1.035
• CP-scar	1.653	2.005	0.255	0.259	1.043
• CutPaste	1.697	2.100	0.258	0.203	1.065
• GEOM	1.754	1.774	0.423	0.446	1.099
• Flip	1.906	2.082	0.257	0.208	1.113
• Color	1.844	2.034	0.336	0.295	1.127
• Invert	2.221	2.116	0.257	0.220	1.204
• Crop	2.143	1.935	0.348	0.424	1.213
• CutOut	1.723	2.066	0.503	0.629	1.230
• Blur	2.182	2.372	0.303	0.221	1.270
• SimCLR	2.074	1.941	0.498	0.582	1.274
• Mask	2.136	2.824	0.585	0.776	1.580
• Noise	4.214	3.170	0.427	0.627	2.110
Identity	2.035	2.402	0.265	0.212	1.228

\mathcal{D}_{gen} . Our observations are consistent with other choices of gen functions as shown in Appendix D.

It is notable from both figures that the augmentation functions of the same category (i.e. the same color) are located together, implying that similar augmentation functions have similar characteristics even though their specifics are different. For example, CutOut works best because it is the perfect match with gen in Fig. 1, while CutPaste and CutPaste-scar still work well since they are in the same category of local augmentations.

5.2 Additional Observations We give additional observations to support our key findings and to better understand the effect of self-supervision on SSAD.

OBSERVATION 1. *Geometric augmentations such as rotation or flipping work best on datasets in which anomalies*



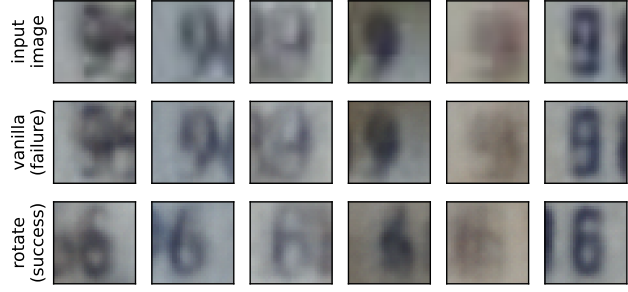
(a) Normal images on CIFAR-10C



(b) Anomalous images on CIFAR-10C



(c) Normal images on SVHN



(d) Anomalous images on SVHN

Figure 5: Images from the CIFAR-10C and SVHN datasets, where the three rows represent original images and those reconstructed by vanilla AE f and DAE f_{aug} , respectively. (a, b) $\text{aug} := \text{CutOut}$ and $\text{gen} := \text{CutOut}$. (c, d) $\text{aug} := \text{Rotate}$, and the digits 6 and 9 are normal and anomalous classes, respectively. The **success** and **failure** represent whether the images are assigned accurately to their true classes (normal vs. anomaly). DAE preserves the original images (on the left) while applying the inverse aug^{-1} of augmentation to anomalies (on the right), making them resemble normal ones with high reconstruction errors. As a result, DAE f_{aug} achieves high AUC of (a, b) 0.986 and (c, d) 0.903, while those of AE f are (a, b) 0.865 and (c, d) 0.549, respectively. See Obs. 3.

lies consist of different semantic classes.

Fig. 4 summarizes results on the in-the-wild testbed of 360 tasks across four datasets and 90 class pairs each, whose anomalies represent different semantic classes in the datasets. The alignment between aug and gen is not known a priori unlike in the controlled testbed.

We observe that geometric augmentation functions such as Rotate and Flip perform best with both models. This is also consistent with the observations in previous works [10, 20], which show the effectiveness of geometric augmentations in detecting semantic class anomalies. One plausible explanation is that many classes in those datasets, such as dogs and cats in CIFAR-10, are sensitive to geometric changes such as rotation. Thus, aug creates plausible samples outside the normal data distribution, giving f_{aug} an ability to differentiate anomalies that may look like augmented normal images.

Table 2 also supports Obs. 1 by measuring MMD between aug functions and class anomalies. Geometric functions including Rotate, Flip, and GEOM show the smallest distances in general, representing that they are more aligned with different semantic classes. A notable difference between Table 2 and Fig. 4 is that SimCLR, which shows large MMD on average, works better than

the local augmentations in Fig. 4b. This is because the large flexibility of augmentation induced by SimCLR is effective for DeepSAD, which learns a hypersphere that encloses normal data separating from pseudo anomalies, while DAE aims to learn exact mappings from pseudo anomalies to normal data in the pixel level.

OBSERVATION 2. *Given a dataset having multiple types of anomalies, aug makes a bias in the error distribution of f_{aug} compared with that of the vanilla f .*

Fig. 2 compares DeepSAD f_{aug} with $\text{aug} := \text{Rotate}$ and its no-SSL baselines, DeepSVDD f , on the multiple types of anomalies on CIFAR-10. We observe that the accuracy of f decreases on Automobile and Truck with aug , which are semantic classes that involve ground (or dirt) and thus can be easily separated from Airplane by unsupervised learning. This is because the supervision with Rotate forces f_{aug} to detect other semantic classes including sky, such as Bird, by feeding rotated airplanes as pseudo anomalies. This result shows that the “bias” phenomenon existing in semi-supervised learning [34] is observed also in SSL, and emphasizes the importance of selecting a proper aug function. We show in Appendix E that the bias is observed also in the DAE model.

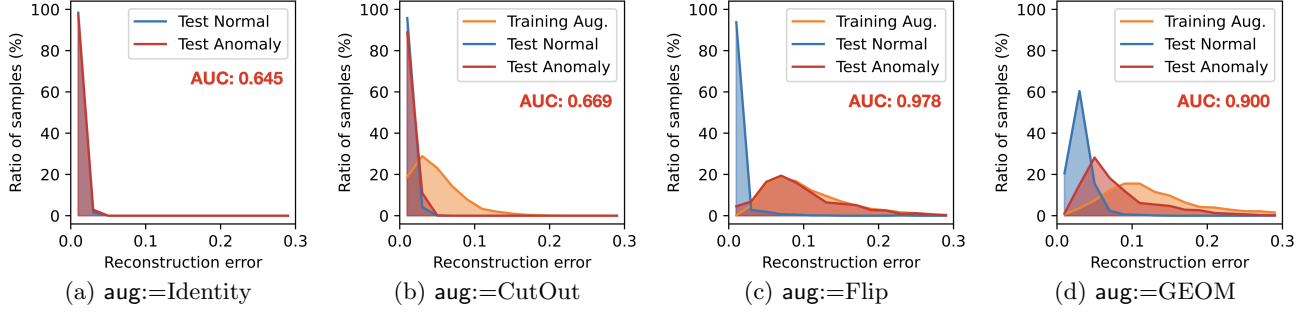


Figure 6: (best in color) Reconstruction error on CIFAR-10C with Automobile as the normal class and $\text{gen} := \text{Flip}$. The distributions gradually shift to the right as the augmentation aug changes the input images more and more: (a) Identity, (b) CutOut (local), (c) Flip (global), and (d) GEOM (“cocktail” augmentation). The distributions of augmented samples and anomalies are matched the most in (c) when $\text{aug} = \text{gen}$, which also achieves the smallest MMD among the four choices of aug functions: (a) 0.063, (b) 0.277, (c) 0.031, and (d) 0.399. See Obs. 4.

6 How Augmentation Works

We perform case studies and detailed analysis to study how augmentation helps anomaly detection. Among the three models, we adopt DAE as the main model of analysis due to the following reasons. First, DAE learns to reconstruct the original sample from its corrupted (in our case, augmented) version, which in effect returns the counterfactual of an anomaly at the output. This helps with the interpretation of actual anomalies at test time. Second, the training of DAE is done by minimizing the reconstruction error without involving sensitive hyperparameters. Finally, DAE supports the *vanilla* version of it, AE, that works *without* augmentation.

6.1 Case Studies We visually inspect individual samples to observe what images DAE reconstructs for normal versus anomalous data. Fig. 5 shows the results on CIFAR-10C and SVHN with different aug .

OBSERVATION 3. *Given a normal example \mathbf{x} , DAE f_{aug} approximates the identity function $f(\mathbf{x}) \approx \mathbf{x}$. Given an anomaly $\text{gen}(\mathbf{x})$, f_{aug} approximates the inverse aug^{-1} if gen and aug are aligned well, i.e., $f_{\text{aug}}(\text{gen}(\mathbf{x})) \approx \mathbf{x}$.*

We observe from Fig. 5 that both DAE and AE produce low reconstruction errors for normal data, but AE fails to predict them as normal since the errors are low also for anomalies. Given anomalies, DAE recovers their counterfactual images by applying aug^{-1} , which is the inverse of aug , increasing their reconstruction errors to become higher than those from the normal images. This allows DAE to achieve higher AUC than AE. We derive the same observation from other pairs of normal classes and anomalies (see Appendix F).

It is noteworthy that the task of detecting digits 9 as anomalous from digits 6 is *naturally aligned* with the Rotate augmentation because, in effect, DAE learns the images of rotated 6 to be anomalies. This is shown also

by the MMD: 0.091 by Rotate, while 0.106 by Identity, where Identity means no augmentation for vanilla f .

6.2 Error Histograms Next, we study the effect of augmentation on the reconstruction error distributions of normal examples and anomalies generated by DAE. Fig. 6 shows the errors histograms on CIFAR-10C.

OBSERVATION 4. *The overall reconstruction errors are higher in DAE f_{aug} than in vanilla AE f , and increase with the degree of change that aug employs.*

We compare DAE with three different aug functions and the vanilla AE in Fig. 6. The DAEs show higher reconstruction errors in general than the AE, providing more right-shifted error distributions. This is because the objective function of DAE involves a denoising term that increases the reconstruction errors for augmented data by mapping them to normal ones. The improved AUC of DAE is the result of increasing reconstruction errors for anomalies than those for normal data.

In Fig. 6, the amount of change incurred by aug increases from Fig. 6a to 6d. The error distributions are shifted to the right accordingly, as augmented data become more different from the normal ones. Notably, the distribution for anomalies is more right-shifted in Fig. 6c than in Fig. 6d, showing higher AUC of 0.978, due to the better alignment between aug and gen . We show in Appendix G that our observation is consistent in different gen functions for various tasks.

6.3 Embedding Visualization Figs. 7 and 8 show data embeddings on CIFAR-10C and CIFAR-10, respectively, learned by DAE with various aug functions.

OBSERVATION 5. *Embeddings from DAE f_{aug} for normal data and anomalies are separated when aug makes global changes, whereas mixed when aug is local.*

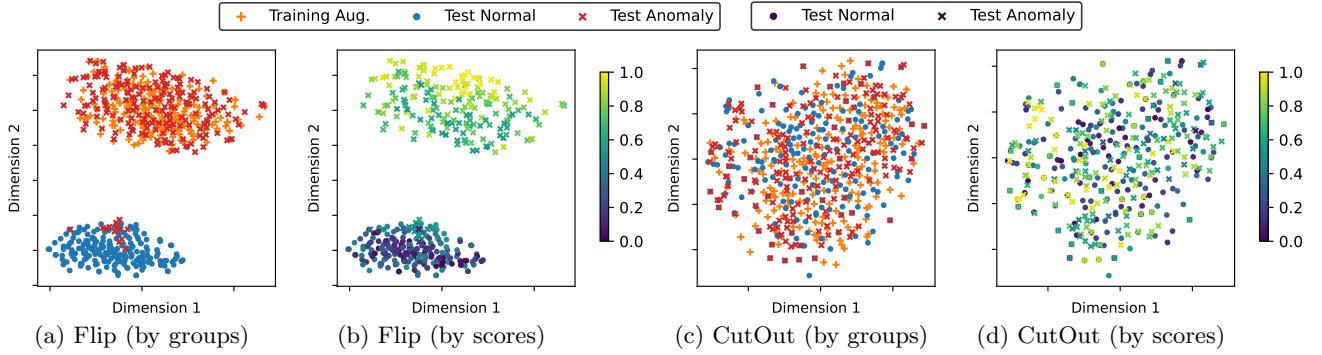


Figure 7: (best in color) t -SNE visualization of embeddings on CIFAR-10C with the perfect alignment ($\text{aug}=\text{gen}$): (a, b) $\text{aug}=\text{gen}=\text{Flip}$ and (c, d) $\text{aug}=\text{gen}=\text{CutOut}$. The colors represent either (a, c) data categories or (b, d) anomaly scores. It achieves high AUC of 0.978 and 0.973 in both cases, respectively, despite the distributions of embeddings being different geometrically: anomalies are either (a, b) separated or (c, d) mixed. See Obs. 5.

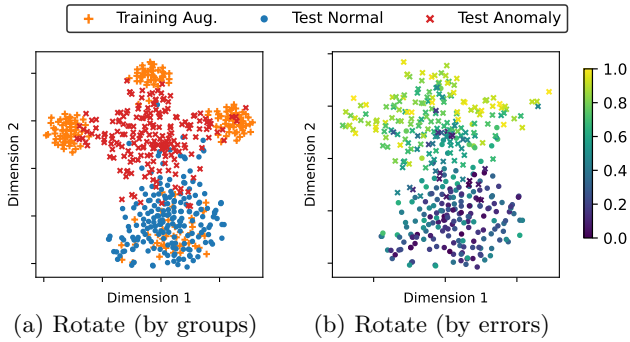


Figure 8: (best in color) t -SNE visualization of embeddings on CIFAR-10 for the task of Automobile (normal) vs. Cat (anomaly). We set $\text{aug}=\text{Rotate}$ in both figures. Colors depict either (a) data categories or (b) anomaly scores. It achieves high AUC of 0.879 even when anomalies are separated from augmented data, while the AUC of vanilla AE is only 0.440. See Obs. 6.

In Fig. 7, The first two and the last two figures exhibit different scenarios. In Figs. 7a and 7b, there are separate clusters: one for normal data, and another for augmented data and anomalies. In Figs. 7c and 7d, all data compose a single cluster without a clear separation between the different categories. The difference between the two scenarios is driven by the characteristic of the aug function: Flip makes global changes in images, while CutOut affects only a part of each image.

OBSERVATION 6. *Augmentation can perform well even under imperfect alignment if the anomalies lie between normal and augmented data in the embedding space.*

Fig. 8 visualizes the result on CIFAR-10 with semantic anomalies and $\text{aug}=\text{Rotate}$. The alignment between aug and gen is not perfect, which is shown by the separation between the augmented data and the anomalies in the embedding space; the augmented points make four separate clusters based on the four degree options

of Rotate , which are $\{0, 90, 180, 270\}$. Nevertheless, the augmentation improves the vanilla AE, since the anomalies lie between normal and augmented data in the embedding space: AUC improves from 0.440 to 0.879. We also show that the observations are consistent in different aug and gen functions on various tasks in Appendix H.

7 Conclusion

In this work, we studied the role of self-supervised learning (SSL) in anomaly detection (AD). Through carefully set-up experiments on three different models across 420 AD tasks, we showed that the alignment between augmentation and anomaly-generating mechanism plays an essential role in the success of SSL; and importantly, SSL may even hurt detection accuracy under poor alignment. As such, SSL for AD emerges as a data-specific solution, rather than a general cure-all panacea, effectively rendering it a model hyperparameter—nontrivial to specify in fully unsupervised settings. Our study is motivated (and our findings are also supported) by various partial evidences reported in previous works, and serves as the first systematic large-scale study to provide comprehensive evidence. We expect our work will trigger future research on a better understanding of this growing area, in addition to principled SSL for AD techniques that can tackle the outlined challenges.

References

- [1] N. ABE, B. ZADROZNY, AND J. LANGFORD, *Outlier detection by active learning*, in KDD, 2006, pp. 504–509.
- [2] S. AKCAY, A. A. ABARGHOUEI, AND T. P. BRECKON, *Ganomaly: Semi-supervised anomaly detection via adversarial training*, in ACCV, 2018.
- [3] L. BERGMAN AND Y. HOSHEN, *Classification-based anomaly detection for general data*, in ICLR, 2020.

[4] T. CHEN, S. KORNLITH, M. NOROZI, AND G. E. HINTON, *A simple framework for contrastive learning of visual representations*, in ICML, 2020.

[5] Z. CHENG, E. ZHU, S. WANG, P. ZHANG, AND W. LI, *Unsupervised outlier detection via transformation invariant autoencoder*, IEEE Access, 9 (2021), pp. 43991–44002.

[6] A. CONNEAU, K. KHANDELWAL, N. GOYAL, V. CHAUDHARY, G. WENZEK, F. GUZMÁN, E. GRAVE, M. OTT, L. ZETTLEMOYER, AND V. STOYANOV, *Unsupervised cross-lingual representation learning at scale*, in ACL, 2020.

[7] J. DEVLIN, M. CHANG, K. LEE, AND K. TOUTANOVA, *BERT: pre-training of deep bidirectional transformers for language understanding*, in NAACL-HLT, 2019.

[8] T. DEVRIES AND G. W. TAYLOR, *Improved regularization of convolutional neural networks with cutout*, CoRR, abs/1708.04552 (2017).

[9] C. DING, G. PANG, AND C. SHEN, *Catching both gray and black swans: Open-set supervised anomaly detection*, CoRR, abs/2203.14506 (2022).

[10] I. GOLAN AND R. EL-YANIV, *Deep anomaly detection using geometric transformations*, in NeurIPS, 2018.

[11] P. GOYAL, M. CARON, B. LEFAUDEUX, M. XU, P. WANG, V. PAI, M. SINGH, V. LIPTCHINSKY, I. MISRA, A. JOULIN, AND P. BOJANOWSKI, *Self-supervised pretraining of visual features in the wild*, CoRR, abs/2103.01988 (2021).

[12] A. GRETTON, K. M. BORGWARDT, M. J. RASCH, B. SCHÖLKOPF, AND A. J. SMOLA, *A kernel method for the two-sample-problem*, in NIPS, B. Schölkopf, J. C. Platt, and T. Hofmann, eds., 2006.

[13] D. J. GROGEL, *Practical nonparametric statistics*, Technometrics, 42 (2000), pp. 317–318.

[14] D. A. GUDOVSKIY, S. ISHIZAKA, AND K. KOZUKA, *CFLOW-AD: real-time unsupervised anomaly detection with localization via conditional normalizing flows*, in WACV, 2022.

[15] K. HE, X. ZHANG, S. REN, AND J. SUN, *Deep residual learning for image recognition*, in CVPR, 2016.

[16] D. HENDRYCKS, M. MAZEIKA, AND T. G. DIETTERICH, *Deep anomaly detection with outlier exposure*, in ICLR, 2019.

[17] A. KRIZHEVSKY, G. HINTON, ET AL., *Learning multiple layers of features from tiny images*, (2009).

[18] Y. LECUN, L. BOTTOU, Y. BENGIO, AND P. HAFFNER, *Gradient-based learning applied to document recognition*, Proc. IEEE, 86 (1998), pp. 2278–2324.

[19] Y. LECUN AND I. MISRA, *Self-supervised learning: The dark matter of intelligence*, 2021.

[20] C. LI, K. SOHN, J. YOON, AND T. PFISTER, *Cutpaste: Self-supervised learning for anomaly detection and localization*, in CVPR, 2021.

[21] Y. NETZER, T. WANG, A. COATES, A. BISSACCO, B. WU, AND A. Y. NG, *Reading digits in natural images with unsupervised feature learning*, (2011).

[22] C. QIU, T. PFROMMER, M. KLOFT, S. MANDT, AND M. RUDOLPH, *Neural transformation learning for deep anomaly detection beyond images*, in ICML, 2021.

[23] M. RUDOLPH, T. WEHRBEIN, B. ROSENHAHN, AND B. WANDT, *Fully convolutional cross-scale-flows for image-based defect detection*, in WACV, 2022.

[24] L. RUFF, N. GÖRNITZ, L. DEECKE, S. A. SIDDIQUI, R. A. VANDERMEULEN, A. BINDER, E. MÜLLER, AND M. KLOFT, *Deep one-class classification*, in ICML, 2018.

[25] L. RUFF, R. A. VANDERMEULEN, N. GÖRNITZ, A. BINDER, E. MÜLLER, K. MÜLLER, AND M. KLOFT, *Deep semi-supervised anomaly detection*, in ICLR, 2020.

[26] T. SHENKAR AND L. WOLF, *Anomaly detection for tabular data with internal contrastive learning*, in ICLR, 2022.

[27] I. STEINWART, D. HUSH, AND C. SCOVEL, *A classification framework for anomaly detection*, JMLR, 6 (2005).

[28] J. TACK, S. MO, J. JEONG, AND J. SHIN, *CSI: novelty detection via contrastive learning on distributionally shifted instances*, in NeurIPS, 2020.

[29] J. P. THEILER AND D. M. CAI, *Resampling approach for anomaly detection in multispectral images*, in Proceedings of the SPIE, vol. 5093, 2003, pp. 230–240.

[30] P. VINCENT, H. LAROCHELLE, Y. BENGIO, AND P. MANZAGOL, *Extracting and composing robust features with denoising autoencoders*, in ICML, 2008.

[31] P. VINCENT, H. LAROCHELLE, I. LAJOIE, Y. BENGIO, AND P. MANZAGOL, *Stacked denoising autoencoders: Learning useful representations in a deep network with a local denoising criterion*, J. Mach. Learn. Res., 11 (2010), pp. 3371–3408.

[32] H. XIAO, K. RASUL, AND R. VOLLGRAF, *Fashion-mnist: a novel image dataset for benchmarking machine learning algorithms*, CoRR, abs/1708.07747 (2017).

[33] F. YE, C. HUANG, J. CAO, M. LI, Y. ZHANG, AND C. LU, *Attribute restoration framework for anomaly detection*, IEEE Trans. Multim., 24 (2022), pp. 116–127.

[34] Z. YE, Y. CHEN, AND H. ZHENG, *Understanding the effect of bias in deep anomaly detection*, in IJCAI, 2021.

[35] S. ZAGORUYKO AND N. KOMODAKIS, in BMVC, 2016.

[36] H. ZENATI, M. ROMAIN, C. FOO, B. LECOUAT, AND V. CHANDRASEKHAR, *Adversarially learned anomaly detection*, in ICDM, 2018.

[37] Z. ZHONG, L. ZHENG, G. KANG, S. LI, AND Y. YANG, *Random erasing data augmentation*, CoRR, abs/1708.04896 (2017).

[38] C. ZHOU AND R. C. PAFFENROTH, *Anomaly detection with robust deep autoencoders*, in KDD, 2017.

[39] B. ZONG, Q. SONG, M. R. MIN, W. CHENG, C. LUMEZANU, D. CHO, AND H. CHEN, *Deep autoencoding gaussian mixture model for unsupervised anomaly detection*, in ICLR, 2018.

A Details on Detector Models

In our experiments, we use the model structures used in previous works. For AE and DAE, we use the structure used in [10]. The encoder and decoder networks consist of four encoder and decoder blocks, respectively. Each encoder block has a convolution layer of 3×3 kernels, batch normalization, and a ReLU activation function. A decoder block is similar to the encoder block, except that the convolution is replaced with transposed convolution of the same kernel size. The number of epochs and the size of hidden features are both set to 256, and the number of convolution features is (64, 128, 256, 512) for the four layers of the encoder block, respectively.

For AP [10] and DeepSAD [25], we use their official implementations for the model structures, optimization, and hyperparameters.²³ The structure of AP is based on Wide Residual Network [35], and DeepSAD is based on a LeNet-type convolutional neural network.

B Augmentation Functions

We provide detailed information on augmentation functions that we study in this work. We use the official PyTorch implementations of augmentation functions and their default hyperparameters when available.

Geometric augmentations modify images with geometric functions:

- Rotate (random rotation) makes a random rotation of an image with a degree in $\{0, 90, 180, 270\}$.
- Crop (random cropping) randomly selects a small patch from an image whose relative size is between 0.08 and 1.0, resizes it to the original size, and uses it instead of the given original image.
- Flip (vertical flipping) vertically flips an image.
- GEOM [10] conducts three types of augmentations at the same time (and in this order): Rotate, Flip, and Translate, where Translate denotes a random horizontal or vertical translation by 8 pixels.

Local augmentations change only a small subset of image pixels without affecting the rest.

- CutOut (random erasing) [8, 37] replaces a small image patch as zero, i.e., black pixels. The patch size is chosen randomly from $(0.02, 0.33)$.
- CutPaste [20] copies a small patch and pastes it into another location in the same image. The difference from CutOut is that CutPaste has no black pixels in resulting images, making them more plausible. The patch size is chosen from $(0.02, 0.15)$.
- CutPaste-scar [20] is a variant of CutPaste, which augments thin scar-like patches instead of rectangular ones. The patch width and height are cho-

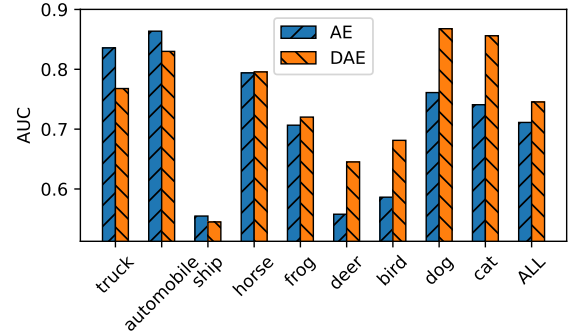


Figure 9: Error distribution comparing DAE with its no-SSL baseline, AE, on CIFAR-10. We set Airplane as the normal class and use Rotate as aug as in Fig. 2. The x-labels represent the types of semantic anomalies. The self-supervision improves the average accuracy (the last column) but impairs accuracy on classes that are easily detected by unsupervised AE. This supports Obs. 2.

sen from $(10, 25)$ and $(2, 16)$, respectively, in pixels. The selected patches are rotated randomly with a degree in $(-45, 45)$ before they are pasted.

Elementwise augmentations make a change in the value of each image pixel individually (or locally).

- Noise (addition of Gaussian noise) [31] is a traditional augmentation function used for denoising autoencoders. It adds a Gaussian noise with the standard deviation of 0.1 to each image pixel.
- Mask (Bernoulli masking) [31] conducts a random trial to each pixel whether to change the value to zero or not. The masking probability is 0.2.
- Blur (Gaussian blurring) [4] smoothens an image by applying a Gaussian filter whose kernel size is 0.1 of the image. The σ of the filter is chosen randomly from $(0.1, 2.0)$ as done in the SimCLR function.

Color augmentations change the color information of an image without changing actual objects.

- Color (Color jittering) [4] makes random changes in the color of an image with brightness, contrast, saturation, and hue. The amount of changes is the same as in the SimCLR function.
- Invert (Color inversion) inverts the color information of an image. In numerical implementation, it returns $1 - x$ for each pixel $x \in [0, 1]$.

Mixed augmentations combine augmentations of multiple categories, making unified changes.

- SimCLR [4] has been used widely in literature as a general augmentation function [28]. It conducts the following at the same time (and in the given order): cropping, horizontal flipping, color jittering, gray scaling, and Gaussian blurring.

²<https://github.com/izikgo/AnomalyDetectionTransformations>

³<https://github.com/lukasruff/Deep-SAD-PyTorch>

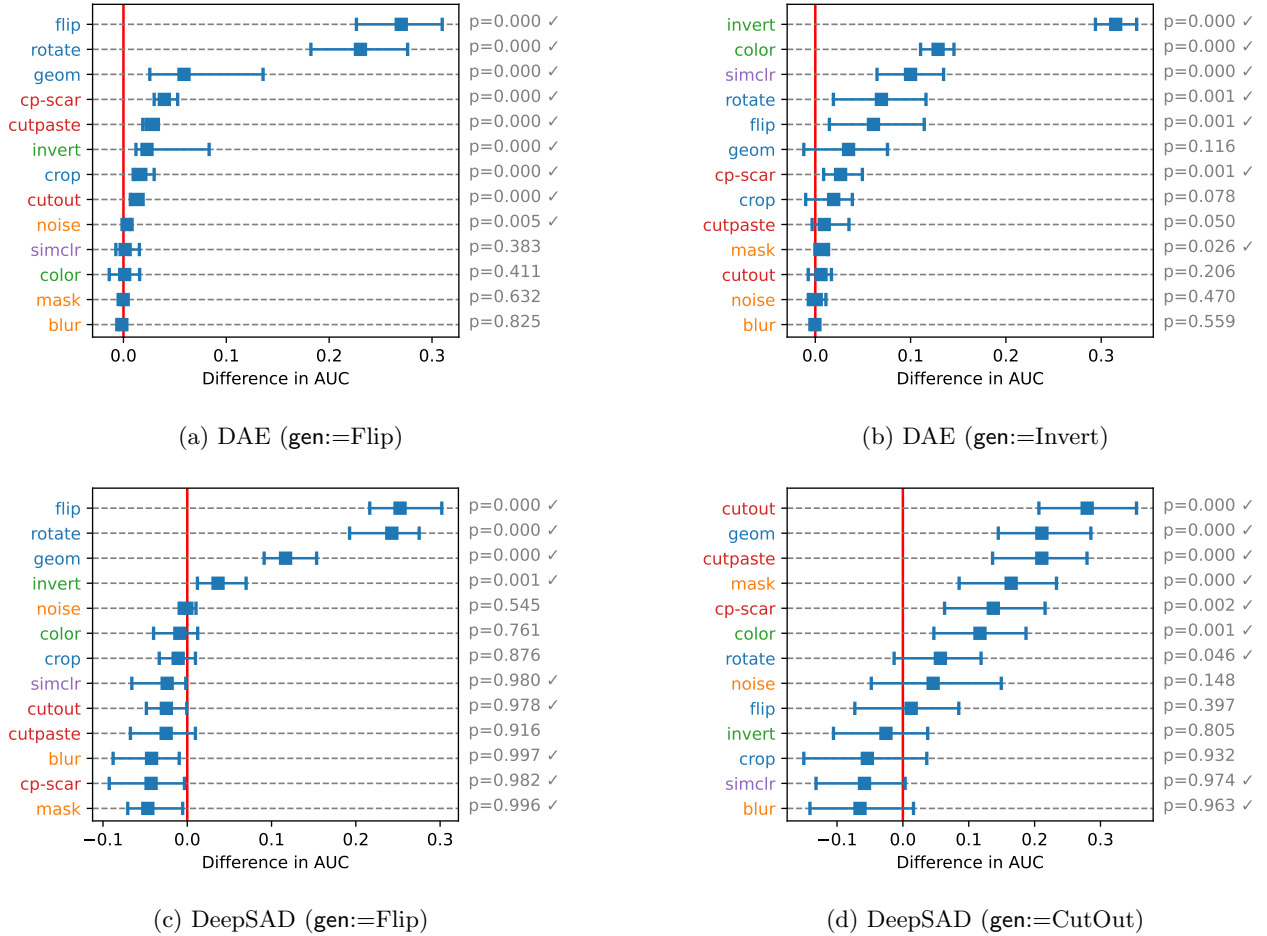


Figure 10: (best in color) Relative AUC of (a, b) DAE and (c, d) DeepSAD with respect to the no-SSL baselines on the controlled testbed with anomaly-generating functions (a, c) $\text{gen}:=\text{Flip}$, (b) $\text{gen}:=\text{Invert}$, and (d) $\text{gen}:=\text{CutOut}$. Color in augmentation names denotes their categories. Augmentation functions that are aligned with the anomaly-generating functions perform well, supporting Key Finding 1 and 2 on the alignment between aug and gen .

C How to Measure MMD Distances

Given an augmentation function aug and an anomaly-generating function gen , we measure the MMD distance between two sets of images generated from aug and gen , respectively, and use it as a measure for their similarity. For each task, such as dogs vs. cats in CIFAR-10, let \mathcal{D} and \mathcal{D}_{gen} be the training and test sets, respectively. \mathcal{D} contains only normal data, while \mathcal{D}_{gen} has both normal data and anomalies, which are generated by gen .

First, we randomly sample M normal samples and anomalies from \mathcal{D} and \mathcal{D}_{gen} , respectively, and represent the results as \mathcal{D}' and $\mathcal{D}'_{\text{gen}}$. Smaller values of M improve efficiency but decrease stability. We set $M = 256$, which is large enough to make stable results. Then, we create $\mathcal{D}'_{\text{aug}} = \{\text{aug}(\mathbf{x}) \mid \mathbf{x} \in \mathcal{D}'\}$ by applying aug to \mathcal{D}' .

The MMD is computed between $\mathcal{D}'_{\text{aug}}$ and $\mathcal{D}'_{\text{gen}}$ as

follows:

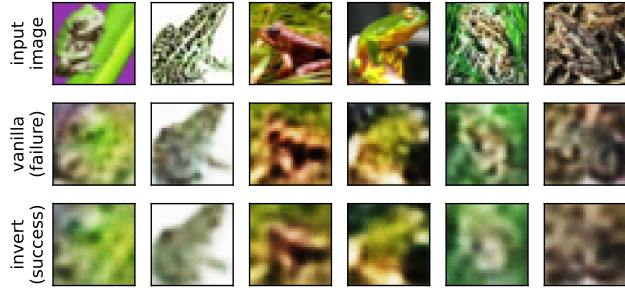
$$\begin{aligned}
 \text{(C.1)} \quad \text{MMD}(\mathcal{D}'_{\text{aug}}, \mathcal{D}'_{\text{gen}}) &= \sum_{\mathbf{x}_1 \in \mathcal{D}'_{\text{aug}}} \sum_{\mathbf{x}_1 \in \mathcal{D}'_{\text{aug}}} k(\mathbf{x}_1, \mathbf{x}_1) \\
 &+ \sum_{\mathbf{x}_2 \in \mathcal{D}'_{\text{gen}}} \sum_{\mathbf{x}_2 \in \mathcal{D}'_{\text{gen}}} k(\mathbf{x}_2, \mathbf{x}_2) - 2 \sum_{\mathbf{x}_1 \in \mathcal{D}'_{\text{aug}}} \sum_{\mathbf{x}_2 \in \mathcal{D}'_{\text{gen}}} k(\mathbf{x}_1, \mathbf{x}_2),
 \end{aligned}$$

where the kernel function $k(\cdot, \cdot)$ is defined on the outputs of a pretrained encoder network ϕ :

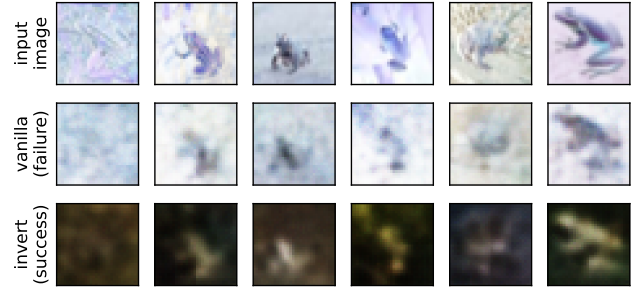
$$\text{(C.2)} \quad k(\mathbf{x}_1, \mathbf{x}_2) = (\gamma \langle \phi(\mathbf{x}_1), \phi(\mathbf{x}_2) \rangle + c)^d.$$

We adopt ResNet50 [15] pretrained on ImageNet as ϕ . The hyperparameters are set to the default values in the scikit-learn implementation: $\gamma = h^{-1}$, $c = 1$, and $d = 3$, where h is the size of embeddings from ϕ .⁴

⁴<https://scikit-learn.org/stable/>



(a) Normal images on CIFAR-10C



(b) Anomalous images on CIFAR-10C



(c) Normal images on SVHN



(d) Anomalous images on SVHN

Figure 11: Images from CIFAR-10C and SVHN, where the three rows represent the original images and those reconstructed by the vanilla AE and DAE, respectively. (a, b) $\text{aug} := \text{gen} := \text{Invert}$. (c, d) $\text{aug} := \text{CutPaste}$, and the digits 0 and 3 are normal and anomalous classes, respectively. The **success** and **failure** represent whether the images are assigned accurately to their true classes based on the computed anomaly scores (normal vs. anomaly). DAE preserves the original images (on the left), while applying the inverse augmentation aug^{-1} to anomalies (on the right), making them resemble normal ones with high reconstruction errors. This allows DAE to achieve higher AUC than AE: (a) 0.996 and (b) 0.651, while those of AE are (a) 0.636 and 0.614. This supports Obs. 3.

D More Results for Key Findings

We present more results of relative AUC on DAE and DeepSAD, supporting Key Finding 1 and 2. We present our findings informally as follows:

- **Finding 1:** DAE works better under better alignment between aug and gen functions.
- **Finding 2:** DAE fails under poor alignment.

Fig. 10 illustrates the results on the controlled testbed across two datasets CIFAR-10C and SVHN-C and ten classes each. Note that the missing combinations, DAE with $\text{gen} := \text{CutOut}$ and DeepSAD with $\text{gen} := \text{Invert}$, are given in the main paper. All four cases presented in the figure with different models and anomaly types support our findings, showing the generalizability of our work.

E More Results for Error Bias

We present an additional analysis of the prediction bias incurred by an augmentation function on DAE. We give our observation informally as follows:

- **Obs. 2:** aug makes a bias in the error distribution of f_{aug} compared with that of the vanilla f .

Fig. 9 shows the error distribution of DAE on CIFAR-10 following the same setting of Fig. 2. We have also the same observation from the result: f_{aug} decreases the accuracy on Automobile and Truck, which are *easy* to detect by the vanilla f , at the expense of improving the general accuracy. This shows that Obs. 2 is consistent in different detector models even with the difference in their characteristics and basic performances.

F More Results on Case Studies

We present more detailed results of case studies, which support Obs. 3 on different types of gen functions. We informally present our observation as follows:

- **Obs. 3:** DAE applies $\text{aug}^{-1}(\cdot)$ to anomalies, while making no changes on normal data.

The four figures in Fig. 11 are divided to the controlled and in-the-wild testbeds. Figs. 11a and 11b show the images of CIFAR-10C when $\text{gen} := \text{Invert}$. DAE applies the inverse augmentation aug^{-1} to the given anomalies, reconstructing normal-like ones by inverting their color back in the reconstructed ones. In contrast, vanilla AE

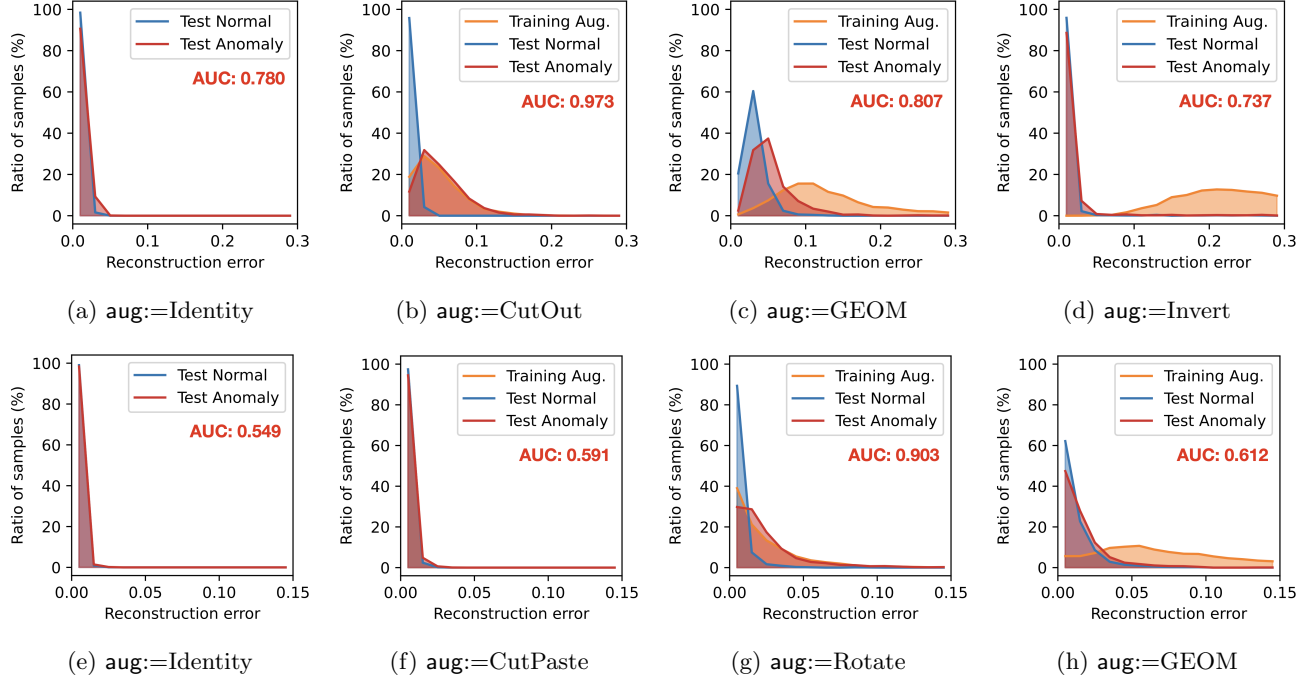


Figure 12: (best in color) Reconstruction errors on (top) CIFAR-10C with Automobile as the normal class and $\text{gen}:=\text{CutOut}$ and (bottom) SVHN for the task of 6 (normal) vs. 9 (anomalous). The distributions gradually shift to the right as the augmentation aug changes the input images more and more. The distributions of augmented samples and anomalies are matched the most in (b) and (g) when $\text{aug} \approx \text{gen}$, consistent with Fig. 6 (see Obs. 4); recall that the gen function in the task of 6 vs. 9 can be thought of approximate Rotate. This is supported also by MMD: (a) 0.228, (b) 0.012, (c) 0.399, (d) 0.251, (e) 0.106, (f) 0.161, (g) 0.091, and (h) 0.471.

reconstructs both normal and anomalous images close to the input, producing low reconstruction errors.

Figs. 11c and 11d present the images from SVHN, in which anomalies are images associated with different numbers, and $\text{aug}:=\text{CutPaste}$. The task is to detect 3 (anomalous) from 0 (normal). The scarred images of 0 can look like the digit 3 by chance. This also makes the alignment between gen and aug by chance, resulting in the partial success of aug ; the improvement of AUC is only 0.037 from the vanilla AE (0.651 vs. 0.614). As a consequence of the (partial) alignment, DAE also shows lower MMD than that of AE: 0.178 vs. 0.249.

G More Results on Error Histograms

We present more detailed results on error histograms to support Obs. 4 on different types of gen functions. We informally present our observation as follows:

- **Obs. 4:** Reconstruction errors are higher in DAE than in AE, increasing with the degree of change.

The four figures in Fig. 12 show the error histograms on controlled and in-the-wild testbeds. The top of Fig. 12 shows the results on CIFAR-10C with $\text{gen}:=\text{CutOut}$. It supports Obs. 4 by presenting the same patterns as in

Fig. 6 even with different gen functions. One notable observation is that the distribution of augmented data is more right-shifted in Invert than in GEOM, even though GEOM is a “cocktail” approach that combines multiple augmentations. This is because Invert changes the value of all pixels simultaneously to invert the whole color of an image, resulting in dramatic pixel-level changes.

The bottom of Fig. 12 shows the error histograms on SVHN adopting different aug functions. The task is 6 (normal) vs. 9 (anomaly), where gen is considered as approximate Rotate; it works best among the four aug options thanks to the best alignment with gen . GEOM makes the most right-shifted distribution of augmented data, as in Fig. 6, because of its “cocktail” nature. This shows that Obs. 4 is valid not only for the controlled testbed but also for the in-the-wild testbed.

H More Results on Embedding Visualization

We introduce more results on embedding visualization on both controlled and in-the-wild testbeds, supporting Obs. 5 and 6 with different aug and gen functions. We informally present our observations as follows:

- **Obs. 5:** Embeddings make separate clusters with

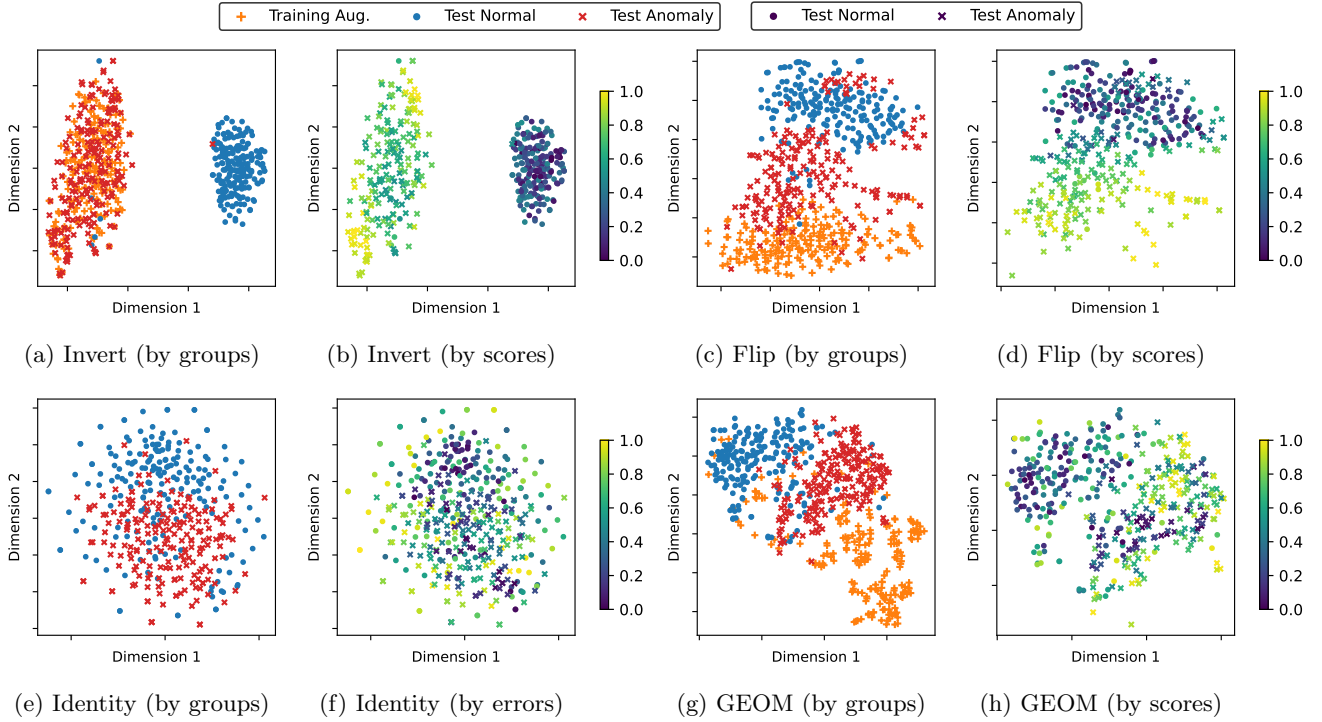


Figure 13: (best in color) t-SNE visualization of data embeddings on (top) CIFAR-10C when Automobile is the normal class and $\text{gen}:=\text{Invert}$: (a, b) $\text{aug}:=\text{Invert}$ and (c, d) $\text{aug}:=\text{Flip}$, and (bottom) CIFAR-10 when the task is Truck (normal) vs. Dog (anomalous): (e, f) $\text{aug}:=\text{Identity}$ and (g, h) $\text{aug}:=\text{GEOM}$. The colors represent either (a, c, e, g) data categories or (b, d, f, h) anomaly scores. We compare the left two and the right two plots, separating into the top and bottom parts. (a, b) $\text{aug}:=\text{Invert}$ creates two separate clusters as claimed in Obs. 5, achieving high AUC of 0.990, due to the perfect alignment with gen (i.e., $\text{aug}=\text{gen}$). (c, d) $\text{aug}:=\text{Flip}$ also achieves high AUC of 0.889, although its alignment with $\text{gen}:=\text{Invert}$ is unclear, since it puts anomalies in between normal and augmented data as claimed in Obs. 6. The bottom part also support Obs. 6. (e, f) The vanilla model creates a single cluster containing both normal and anomalous data, and higher anomaly scores are observed for the data outside the cluster. (g, h) On the other hand, GEOM makes a separate cluster for each category of data, putting anomalies in between normal and anomalous data; it results in improved AUC (0.701 vs. 0.494).

global aug , and are mixed with local aug .

- **Obs. 6:** aug performs effectively when anomalies lie between normal and augmented data.

The top of Fig. 13 presents the results on CIFAR-10C with $\text{gen}:=\text{Invert}$ and two aug functions. In Figs. 13a and 13b, when $\text{aug}:=\text{Invert}$ makes the perfect alignment with gen and induces global changes in the image pixels through augmentation, the data make separate clusters supporting Obs. 5 and result in AUC of 0.990. In Figs. 13c and 13d, when $\text{aug}:=\text{Flip}$ whose alignment with gen is imperfect, it still achieves high AUC of 0.889, since it succeeds in putting the anomalies in between normal and augmented data in the embedding space. It allows f to effectively detect anomalies as claimed in Obs. 6.

The bottom of Fig. 13 compares the vanilla AE and DAE with $\text{aug}:=\text{GEOM}$ on CIFAR-10. The vanilla AE in Figs. 13e and 13f creates a single cluster containing

both normal samples and anomalies. Its AUC is 0.494, which is worse than a random guess. On the other hand, DAE in Figs. 13g and 13h creates separate clusters for normal data and anomalies. The augmented data reside in a cluster that is separate from both normal data and anomalies due to the unclear (or unknown) alignment between aug and gen . Still, DAE achieves high AUC of 0.701, because it puts the anomalies in between normal and augmented data. This supports Obs. 6.